Acta Pharmaceutica Sinica B 2022;12(6):2845–2858

Chinese Pharmaceutical Association
Institute of Materia Medica, Chinese Academy of Medical Sciences

Acta Pharmaceutica Sinica B

www.elsevier.com/locate/apsb
www.sciencedirect.com

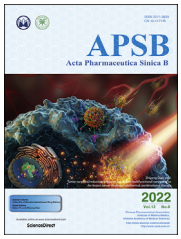

ORIGINAL ARTICLE

YPD-30, a prodrug of YPD-29B, is an oral small-molecule inhibitor targeting PD-L1 for the treatment of human cancer

Fangfang Lai[a,†], Ming Ji[a,†], Lei Huang[a], Yunchen Wang[a], Nina Xue[a], Tingting Du[a], Kai Dong[c], Xiaoqing Yao[c], Jing Jin[a,*], Zhiqiang Feng[b,*], Xiaoguang Chen[a,*]

[a]*Department of Pharmacology, State Key Laboratory of Bioactive Substances and Functions of Natural Medicines, Institute of Materia Medica, Chinese Academy of Medical Sciences and Peking Union Medical College, Beijing 100050, China*
[b]*Department of Pharmacochemistry, Institute of Materia Medica, Chinese Academy of Medical Sciences and Peking Union Medical College, Beijing 100050, China*
[c]*Tianjin Chase Sun Pharmaceutical Co., Ltd., Tianjin 300170, China*

Received 29 October 2021; received in revised form 13 December 2021; accepted 17 February 2022

KEY WORDS

PD-L1;
Small molecular inhibitor;
Prodrug;
Immune checkpoints;
Cancer immunotherapy

Abstract PD-1 and PD-L1 antibodies have brought about extraordinary clinical benefits for cancer patients, and their indications are expanding incessantly. Currently, most PD-1/PD-L1 agents are administered intravenously, which may be uncomfortable for some cancer patients. Herein, we develop a novel oral-delivered small molecular, YPD-29B, which specifically targets human PD-L1. Our data suggested that YPD-29B could potently and selectively block the interaction between PD-L1 and PD-1, but did not inhibit any other immune checkpoints. Mechanistically, YPD-29B induced human PD-L1 dimerization and internalization, which subsequently activated T lymphocytes and therefore overcomes immunity tolerance *in vitro*. YDP-29B was modified as the YPD-30 prodrug to improve druggability. Using humanized mice with human PD-1 xenografts of human PD-L1 knock-in mouse MC38 cancer cells, we demonstrated that YPD-30 exhibited significant antitumor activity and was well tolerated *in vivo*. Taken together, our results indicate that YPD-30 serves as a promising therapeutic candidate for anti-human PD-L1 cancer immunotherapy.

*Corresponding authors. Tel./fax: +86 10 863165207.
E-mail addresses: rebeccagold@imm.ac.cn (Jing Jin), fengzhq@imm.ac.cn (Zhiqiang Feng), chxg@imm.ac.cn (Xiaoguang Chen).
†These authors made equal contributions to this work.
Peer review under responsibility of Chinese Pharmaceutical Association and Institute of Materia Medica, Chinese Academy of Medical Sciences.

https://doi.org/10.1016/j.apsb.2022.02.031

1. Introduction

Cancer immunotherapy is a breakthrough for cancer therapy, changing the landscape of cancer treatment not only by prolonging the overall survival of cancer patients, but also by improving the quality of life[1]. Currently, the most successful immunotherapies include immune checkpoint inhibitors and chimeric antigen receptor (CAR) T-cell therapies[2]. Anti-human cytotoxic T lymphocyte antigen 4 (CTLA4) antibody was the first immune checkpoint inhibitor to be officially approved by the U.S. Food and Drug Association (FDA), followed by anti-programmed death protein 1 (PD-1)/programmed death-ligand 1 (PD-L1) antibodies[3]. As the pronounced therapeutic effects of these immune checkpoint inhibitors have been repeatedly reported in different clinical trials, the indications of these immunotherapy drugs are now expanding to melanoma, skin cancer, bladder cancer, head and neck cancer, lung cancer, lymphoma, gastric cancer, pancreatic cancer[4] and urothelial carcinoma. Furthermore, anti-PD-1 antibody can also be used in the treatment of patients with unresectable or metastatic tumors with high microsatellite instability (MSI-H), or mismatch repair deficient tumors[5,6]. More importantly, immune checkpoint inhibitors have been shown to combine with other therapies such as chemotherapy to bring synergistically prognostic advantages to cancer patients. Therefore, many clinical trials are currently underway to investigate more indications and particularly anti-PD-1/PD-L1 antibodies[7,8].

Although the available clinical immune checkpoint inhibitors showed great antitumor activities including immune-related adverse events, a low response rate, and limitations in intravenous administration[9,10] to overcome such shortcomings, small inhibitors targeting the immune checkpoint interaction that can be administered orally are emerging as a novel strategy for immunotherapy[11–15]. For example, CA-170 developed by the Curis, Inc. is the first small oral inhibitor tested in a human clinical trial targeting VISTA and PD-L1[16], and the Phase I results already suggest antitumor activity of CA-170 including tumor shrinkages and stabilized disease progression. Our compound YPD-29B is a small molecule non-peptide compound that directly targets PD-L1. Compared the PD-1/PD-L1 antibody or peptide, such as CA-170, the molecular weight of YPD-30 is relatively small. Thus, it exhibits significant advantages, with improved oral administration, high stability, membrane permeability, and non-immunogenicity. The disadvantage of YPD-30, compared to other small-molecule drugs, is that its molecular weight is relatively large, which may affect its solubility and membrane permeability. YPD-30, which was designed as a prodrug for the potent PD-1/PD-L1 inhibitor YPD-29B, is currently in a phase I clinical trial in China. As the first small molecule compound PD-L1 in clinical trials in China, we believe that YPD-30 will achieve great success in the treatment of lung cancer.

In this study, our objective was to develop a potent and selective small molecular human PD-L1 inhibitor and to evaluate its therapeutic potential for cancer therapy using both *in vivo* and *ex vivo* models.

2. Materials and methods

2.1. Cell line

The hPD-L1 MC38 cell line was purchased from Nanjing Galaxy Biopharma Co., Ltd. (Nanjing, China) and was cultured in Gibco RPMI 1640 medium (Thermo Fisher Scientific, Waltham, MA, USA) containing 10% Gibco FBS (Thermo Fisher Scientific), 100 μg/mL hygromycin B (InvivoGen, Pak Shek Kok, Hong Kong, China), and 100 IU/mL penicillin/streptomycin (Livning Biological Technology Co., Ltd., Beijing, China). Cells were kept in a humidified incubator at 37 °C with 5% CO_2.

2.2. PD-1/PD-L1 binding assay with homogeneous time-resolved fluorescence

The PD-1/PD-L1 binding assay was performed with the human PD-1/PD-L1 binding assay kit (Cisbio, Codolet, France) according to the manufacturer's instructions. Briefly, 2 μL of compound/antibody or diluent (vehicle control), 4 μL of 25 nmol/L Tag1-PD-L1 protein, and 4 μL of 250 nmol/L Tag2-PD-1 protein were mixed in a white 384-well plate for 15 min at room temperature. Next, 10 μL of premixed anti-Tag1-$Eu3^+$ and anti-Tag2-XL665 were dispersed in the wells. After 2 h of incubation, the homogeneous time-resolved fluorescence (HTRF) signal was detected by the EnSpire microplate reader (PerkinElmer, MA, USA) and calculated using Eq. (1):

$$\text{HTRF ration} = \text{Signal 665 nm/Signal 615 nm} \times 10^4 \quad (1)$$

2.3. Surface plasmon resonance analysis

Surface plasmon resonance (SPR) was used to determine binding affinity with the PD-L1 protein was carried out on Biacore T200 instruments using NTA sensor chips (GE Healthcare Life Sciences, Marlborough, MA, USA). First, 5 μg/mL PD-L1 protein was immobilized on the surface of the sensor chip to reach 1500 RU for the compound assay or 10 RU for the antibody assay, note that one of the four flow cells on the chip was left free as a negative control. Compounds at different concentrations were injected into the surface of the sensor chip for association analysis, followed by dissociation analysis. All data were obtained at 25 °C with running buffer HBS-P (10 mmol/L HEPES, 150 mmol/L NaCl and 0.005% (*v*/*v*) surfactant P20, pH 7.4) and 0.01% dimethyl sulfoxide (DMSO). The equilibrium dissociation constant (K_D) was determined by steady-state fitting mode with Biacore T200 Evaluation Software, version 2.

2.4. Flow cytometry assay

The hPD-L1 MC38 cells were cultured in 12-well plates and exposed to various concentrations of compounds for 24 h. The cells were then digested with trypsin and then collected. Blood samples were treated with red blood cell lysate (Solarbio Life Sciences, Beijing, China) to remove red blood cells according to the manufacturer's recommended procedures. For the tumor tissues, the tumors were minced with scissors and then homogenized with a homogenizer to prepare a single cell suspension. The red

blood cells in the cell suspension were lysed by the same method described above. All cells were incubated with fluorescence labeled antibodies for 1 h at room temperature (RT) and then washed with phosphate-buffered saline (PBS) for 3 times. The ratio or fluorescence intensity of the required cells was determined by flow cytometry (BD Verse, New Jersey, USA).

2.5. *Immunoblotting analysis*

The method was adapted according to the previous report[17]. Briefly, tumor tissues were collected and lysed in lysis buffer containing 1% sodium dodecyl sulfate (SDS), 10 mmol/L ethylenediaminetetraacetic acid, 50 mmol/L Tris-HCl (pH 8.1), and 1% protease inhibitor mixture (Sigma−Aldrich, MO, USA). The lysates were then centrifuged at 13,000 rpm (Thermo Fisher Scientific) for 10 min and the supernatants were collected. Protein concentrations were determined using the BCA protein assay kit (Beyotime biotechnology, Shanghai, China). In total, 60 μg protein samples were loaded and separated by 10% SDS polyacrylamide gel electrophoresis and transferred to a nitrocellulose membrane using semi-wet electrophoresis. The membranes were blocked with 3% fat free dry milk in Tris-buffered saline-Tween 20 (TBS-T) and then incubated overnight with primary antibodies (1:1000 dilution) at 4 °C. After washing three times with TBS-T, the membranes were

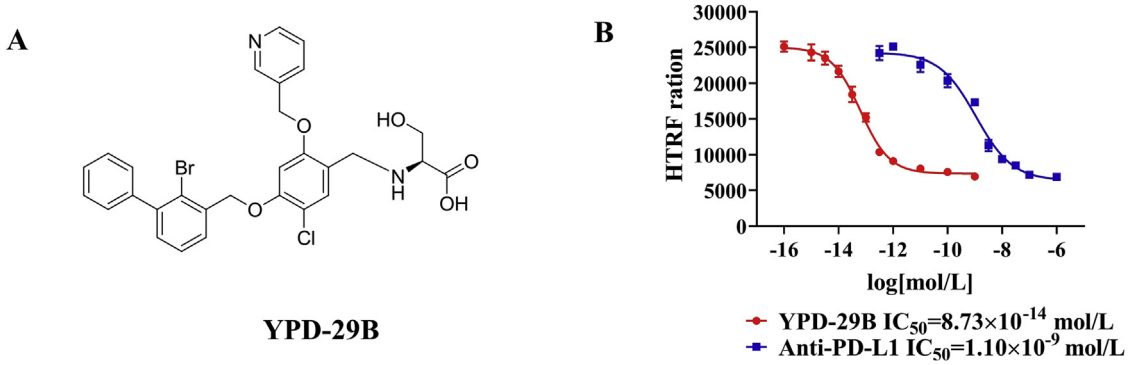

C

	k_a (1/mol·L^{-1}·s)	k_d (1/s)	K_D (mol/L)
YPD-29B	1.529×10^{6}	5.603×10^{-5}	3.666×10^{-11}
Anti-PD-L1	3.283×10^{6}	2.818×10^{-4}	8.584×10^{-11}

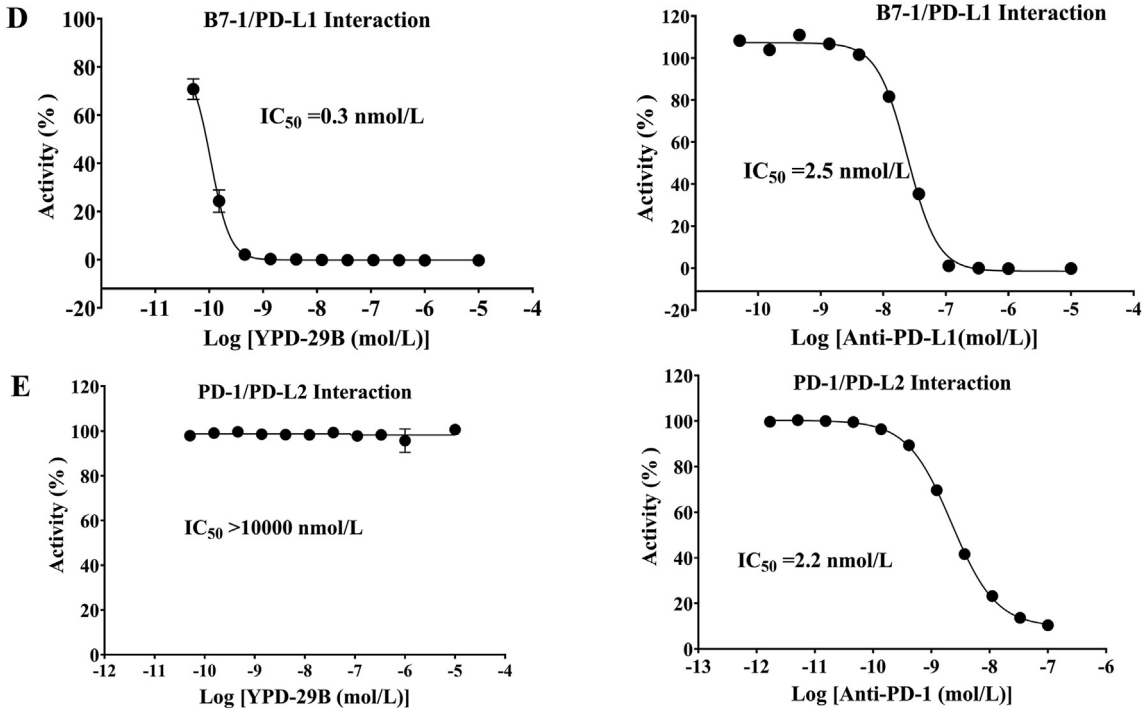

Figure 1 The chemical structure of YPD-29B and its activity *in vitro*. (A) Chemical structure of YPD-29B. (B) YPD-29B disturbs the hPD-1/hPD-L1 interaction as shown by the HTRF assay. The PD-L1 neutralizing antibody acts as the positive control. The assays were performed in duplicate at each concentration. (C) The specific K_D value of YPD-29B by the SPR method. k_a, association rate constant; k_d, dissociation rate constant; K_D, equilibrium dissociation constant (k_d/k_a). (D) YPD-29B blocks the hB7-1/hPD-L1 interaction as determined by ELISA. hPD-L1 neutralizing antibody acts as the positive control. The assays were performed in duplicate at each concentration. (E) YPD-29B has no effect on hPD-1/hPD-L2 interaction by ELISA. hPD-1 neutralizing antibody is a positive control. The assays were performed in duplicate at each concentration.

Table 1 The selectivity of YPD-29B on different immune checkpoints.

Immune checkpoint	IC_{50} (nmol/L)	
	YPD-29B	Positive control
hPD-1/hPD-L1	0.32	2.2 (PD-1 antibody)
hB7-1/hPD-L1	0.3	2.5 (PD-L1 antibody)
mPD-1/mPD-L1	>10,000	2.7 (mPD-L1 antibody)
hPD-1/hPD-L2	>10,000	2.2 (PD-1 antibody)
hCD28/hB7-1	>10,000	7.8 (CTLA4 Fc)
hCD28/hB7-2	>10,000	13 (CTLA4 Fc)
hCTLA4/hB7-1	>10,000	2.8 (CTLA4 antibody)
hCTLA4/hB7-2	>10,000	5.3 (CTLA4 antibody)
LAG3/MHC II[a]	>10,000	30 (LAG3 antibody)

[a]HTRF.

incubated with secondary antibodies (1:1000) for 1 h. The blots were visualized using a chemiluminescence detection kit (BIO-RAD, Hercules, CA, USA) using Image Quant LAS 4000 (GE Healthcare, Marlborough, MA, USA).

2.6. Protein−protein interaction assay

The effects of the compounds on protein−protein interaction including hPD1-hPD-L1, hPD-L1-hB7-1, hPD1-hPD-L2, hCD28-hB7-1, hCD28-hB7-2, hCTLA4-hB7-1, hCTLA4-hB7-2, and mPD1-mPD-L1 were analyzed by the BPS Bioscience company (San Diego, CA, USA). Briefly, the ligand protein was coated with 50 μL at 2−5 ng/mL at 4 °C overnight. Test compounds or neutralizing antibodies were added to the coated plate followed by the addition of the receptor protein biotin. The reaction was incubated for 2 h at room temperature. Binding assays were performed in duplicate at each concentration. The luminescence data were analyzed using the computer software, GraphPad Prism (GraphPad Software, San Diego, CA, USA).

2.7. Homogeneous time-resolved fluorescence-based dimerization assay for PD-L1

For the homogeneous time-resolved fluorescence (HTRF)-based dimerization assay, 200 nmol/L His-tag hPD-L1 protein (Acro-Biosystems, Beijing, China), 60 nmol/L FC-tag PD-L1 protein with or without test compounds were incubated in a black 384-well polystyrene plate for 30 min at room temperature. Then 10 μL of HTRF detection buffer supplemented with Europium cryptate-labeled anti-hIGg (PerkinElmer, MA, USA) specific for Fc and anti-His antibody conjugated to Allophycocyanin (PerkinElmer, MA, USA) were added to the wells for 2 h. The HTRF signal was detected by the EnSpire microplate reader (PerkinElmer, MA, USA). The HTFR ratio and dimerization are calculated as Eqs. (1) and (2), respectively:

$$\text{Dimerization} = \text{the HTRF ratio with compound/the HTRF ratio of control} \quad (2)$$

2.8. Native page assay for PD-L1 protein dimerization

hPD-L1 protein (0.1 μg/μL) (Sino Biological, Beijing, China) and different concentrations of compounds were incubated in a tube for 2 h. The samples were then separated by polyacrylamide gel electrophoresis without SDS. The gel was photographed after staining with Coomassie brilliant blue (Sino Biological, Beijing, China).

2.9. PD-L1 cell-based assay

The activity of compounds in the PD-L1 cell-based assay was determined by the BPS Bioscience Company (San Diego, CA, USA) using a kit. Briefly, 100 μL TCR activator/PD-L1 CHO cells were seeded at a density of 35,000 cells per well in a 96-well white clear bottom microplate. After 24 h, the media was removed from the TCR/PD-L1 CHO cells and 50 μL/well of diluted compounds or control antibody was added. After a 30-min of incubation, 2×10^4 PD-1/NFAT reporter-Jurkat cells were added to the CHO cells. After 5−6 h, cells were lysed and a luciferase assay was performed using the ONE-Step luciferase assay system (BPS Bioscience Company, San Diego, CA, USA). Luminescence was measured using a luminometer (BioTek Synergy™ 2 microplate reader, Winooski, VT, USA).

2.10. Peripheral blood mononuclear cell−cell activation assay

Lectin from *Phaseolus vulgaris* (PHA), hPD-L1 protein (Sino Biological, Beijing, China), and PD-L1 antibody (Bio X Cell, Lebanon, NH, USA), or compounds were added to primary human T cell cultures (HemaCare, Los Angeles, CA, USA) for 3 days. The final concentration of PHA was 1 μg/mL and hPD-L1 was 5 μg/mL. The release of interferon-gamma (IFN-γ) in the media was measured by IFN-γ Human Simple Step ELISA Kit (Abcam, Waltham, MA, USA). Briefly, the cell supernatant was diluted 5 times with the sample dilution solution. Next, 50 μL of standard or test sample was added to each well in the ELISA plate, and 50 μL of antibody mixture was added to each well and incubated on a shaker at RT for 1 h. The cells were rinsed 3 times with wash buffer, and 100 μL TMB solution was added to the wells and incubated on the shaker for 10 min. Finally, 100 μL stop solution was added to each well and the absorbance OD value was measured at 450 nm.

2.11. Immunofluorescence and immunohistochemical staining

A total of 2.5×10^5 hPD-L1 MC38 cells were seeded in 35-mm glass bottom cell culture plates (Nest Scientific, Rahway, NJ, USA). After treating cells with YPD-29B for 24 h, cells were fixed and permeabilized, then incubated with anti-PD-L1 (Cell Signaling Technologies, Danvers, MA, USA) overnight. After washing, cells were stained with goat anti-mouse IgG conjugated to Alexa Fluor Plus 488 (Thermo Fisher Scientific) and cell nuclei were stained with DAPI (Thermo Fisher Scientific). Finally, the cells were observed and analyzed with a Zeiss LSM 710 confocal microscope (Carl Zeiss, Oberkochen, Germany). For immunohistochemical staining, formalin-fixed tumors were embedded in paraffin and cut into slides. The 4-μm sections were then incubated with the primary antibodies anti-CD3, anti-CD8a, and anti-hPD-L1 (Abcam, Cambridge, UK) overnight. After washing, the tumors were stained with a DAB Quanto Kit (Golden Bridge Biological Technology, Beijing, China) and photographed.

2.12. Animal studies

All animal experiments were approved by the Animal Care and Use Committee of the Institute of Materia Medica, Chinese Academy of Medical Sciences, and Peking Union Medical College (Beijing, China). Five-to six-week-old female hPD-1 C57BL/6 mice were obtained from the Nanjing Biomedical Research Institute of Nanjing University (Nanjing, China). hPD-L1 MC38 cell lines were cultured and harvested in saline. A total of 5×10^5 cells were injected subcutaneously into the right flank of the mice. When the

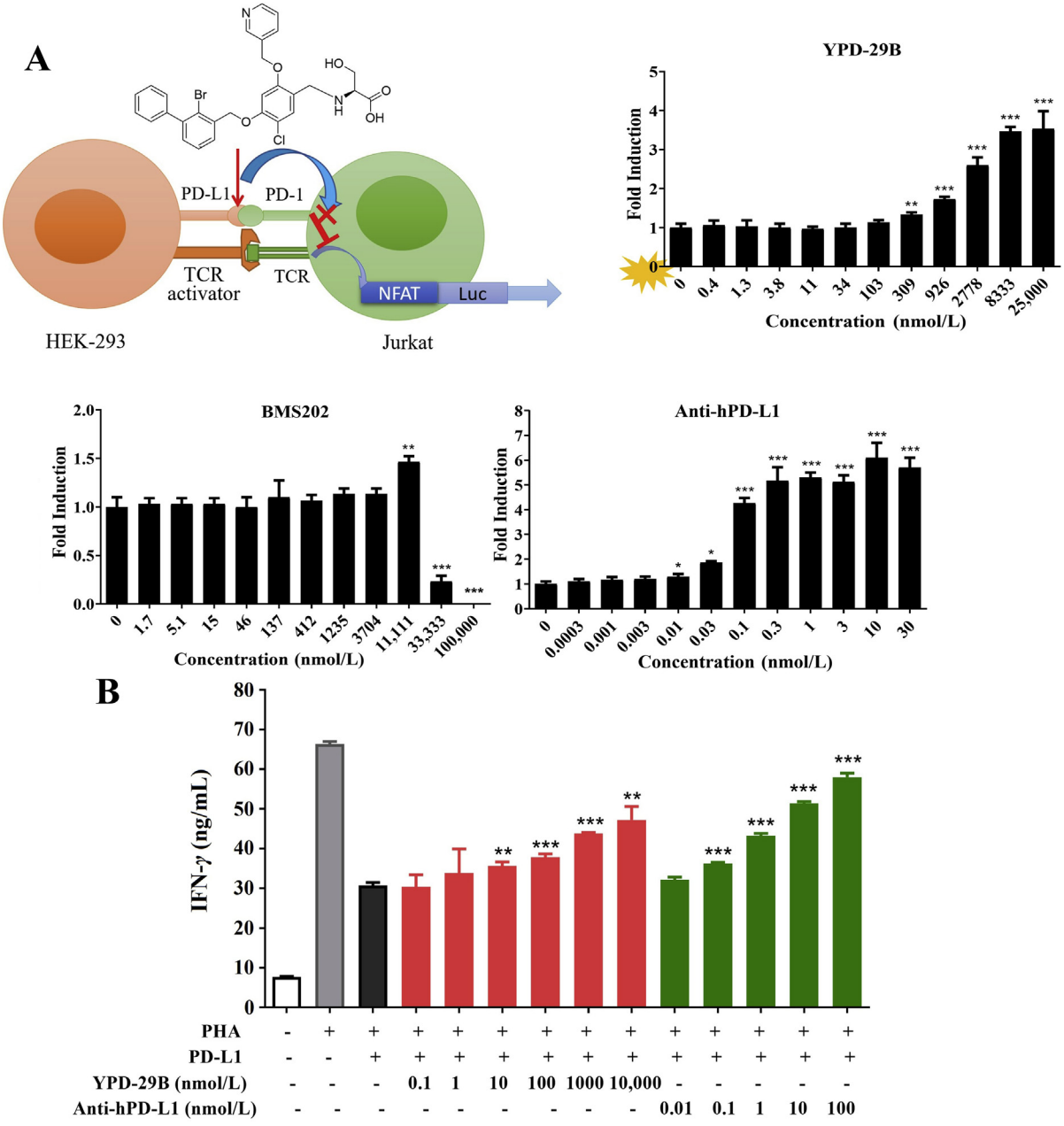

Figure 2 The effects of YPD-29B on T lymphocyte activation. (A) YPD-29B activates the PD-1/NFAT reporter-Jurkat cells. TCR Activator/PD-L1 CHO cells were seeded first, then next day the compounds or antibody were added to the cells. After 30-min incubation, the PD-1/NFAT reporter-Jurkat cells were added to the CHO cells. After 5 h incubation, luciferase assay was determined by ONE-Step luciferase assay system in triplicate at each concentration. (B) YPD-29B rescues IFN-γ expression in human PBMC cells from PD-L1 inhibition. 3×10^5/well PBMC cells were stimulated by 5 μg/mL PHA and then exposed to 1 μg/mL hPD-L1 protein. The IFN-γ concentration was determined by ELISA assay. The assays were performed in triplicate at each concentration. Data are presented as mean ± SD, $^*P < 0.05$, $^{**}P < 0.01$, $^{***}P < 0.001$ *vs*. indicated, data is analyzed using Student's *t*-test.

average tumor volume reached 100−200 mm^3, the mice were randomly enrolled in the control and experimental groups ($n = 7$) and treatment was started on Day 1. For the control group, 0.5% (*w*/*v*) sodium carboxymethyl cellulose Na (CMCNa) was administered orally every day. YPD-30, a prodrug for YPD-29B with significantly higher bioavailability than YPD-29B, was dissolved in 0.5% CMCNa for oral treatment every day and anti-PD-L1 antibody (Bio X Cell, Lebanon, NH, USA) was dissolved in saline for intraperitoneal treatment twice a week. Tumor volumes were measured twice a week. At the end of the experiment, the mice were sacrificed and the tumors were collected, weighted, and analyzed. The tumor volume was calculated as Eq. (3):

$$V = 1/2 \times L \times W^2 \tag{3}$$

in which L is the maximum tumor length and W is the maximum tumor width. Tumor growth inhibition (TGI) was calculated as Eq. (4):

$$\text{TGI} = (1 - \text{Tumor weight of treatment group/Tumor weight of vehicle group}) \times 100\% \tag{4}$$

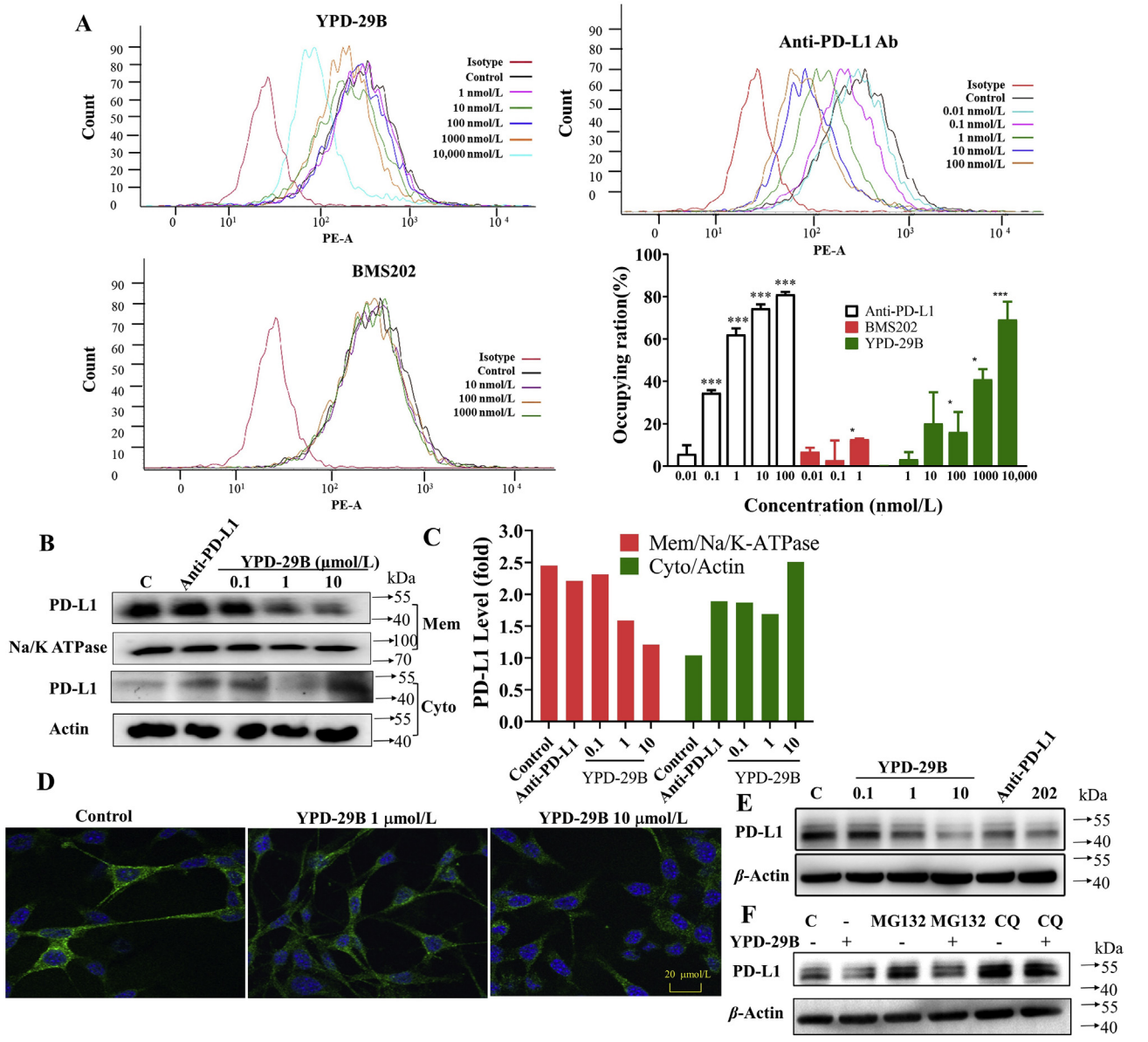

Figure 3 YPD-29B binds to hPD-L1 and the hPD-L1 is then internalized. (A) The PD-L1 protein is bound by YPD-29B on the cell surface. The hPD-L1 MC38 cells were treated with anti-PDL1 antibody (10 nmol/L), BMS202 (10 μmol/L), and YPD-29B (0.1, 1, 10 μmol/L) for 24 h. The cells were collected and stained for PE-marked-hPD-L1. The cell surface expression of PD-L1 was determined by flow cytometry. The combined data at least triplicates were shown. Occupancy ratio = (MFI of Control − MFI of Treated group)/(MFI of Control − MFI of blank group) × 100%, MFI (Median Fluorescence Intensity). Data are presented as mean ± SD, (n = 3); *P < 0.05, **P < 0.01, ***P < 0.001 *vs.* indicated, data is analyzed using Student's t-test. (B) YPD-29B induces PD-L1 protein internalization. After a 24-h treatment, the PD-L1 protein present in the cytoplasm (Cyto) and membrane (Mem) fractions of the cells were determined by Western blotting and a representative image is shown. Na/K-ATPase and β-actin are loading as controls, respectively. (C) Statistical analysis of the Western blotting findings in (B). The densitometric analysis of the bands was determined by Image J. Statistical analysis was used to compare each YPD-29B treated group and the control group. (D) The internalization and localization of hPD-L1 is determined by immunostaining. The hPD-L1 MC38 cells were treatment with 1 and 10 μmol/L YPD-29B for 24 h. Then the cells were immunostained with hPD-L1 antibody (green) and the nuclei were stained with DAPI (Blue). Scale bar = 20 μm. (E) YPD-29B induces total PD-L1 degradation. hPD-L1 MC38 cells were treated with 0.1, 1, and 10 μmol/L of YDP-29B for 24 h. Then the whole cells are collected for Western blotting. (F) YPD-29B induces PD-L1 degradation through the lysosome pathway. The hPD-L1 MC38 cells were treated with 5 μmol/L MG132 or 100 μmol/L chloroquine for 1 h, then followed by treatment with 10 μmol/L YPD-29B for 24 h. Then the whole cells are collected for Western blotting.

2.13. Statistical analysis

Statistical analysis was performed with GraphPad Prism 8.0 software and the significance level was evaluated with one-way ANOVA.

3. Results

3.1. Development of YPD-29B as a potent and selective inhibitor targeting PD-L1

To develop a potent and selective inhibitor targeting hPD-1/hPD-L1, we screened a small pool of molecular compounds to evaluate their inhibitory effect on the interaction of PD-1 and PD-L1 by the HTRF assay. Among these compounds, YPD-29B (Fig. 1A) showed strong inhibitory activity in human PD-1 (hPD-1) and PD-L1 (hPD-L1) interaction with an IC_{50} value of 0.087 pmol/L, while the IC_{50} for the neutralized antibody of hPD-1 was 1.1 nmol/L (Fig. 1B). To investigate whether YPD-29B binds to hPD-1 or hPD-L1, we first detected the K_D value of YPD-29B with the recombinant PD-L1 protein using the SPR method. The K_D value of YPD-29B was 2.03×10^{-11} mol/L, compared to 6.74×10^{-10} mol/L for the hPD-L1 antibody (Fig. 1C and Supporting Information Fig. S1), but YPD-29B did not interact with the hPD-1 protein (data not shown). Since the functional ligands of PD-1 also include B7-1, we also examined the disrupted effect of YPD-29B on the interaction between hPD-L1 and B7-1. Interestingly, YPD-29B also suppressed the interaction of hPD-L1/hB7-1 with an estimated IC_{50} value of 0.3 nmol/L, compared to 2.5 nmol/L for the IC_{50} value of the PD-L1 antibody (Fig. 1D). Furthermore, since hPD-L2 shares some homology with PD-L1, we also evaluated the effects of YPD-29B on the interaction of hPD-1/hPD-L2. Our data suggest that YPD-29B did not show any inhibitory effect on the hPD-1/hPD-L2 interaction (Fig. 1E). These data demonstrate that YPD-29B was a potent small molecular inhibitor targeting hPD-L1 *in vitro*.

Next, to examine whether YPD-29B was a specific hPD-L1 checkpoint inhibitor, we investigated its effects on different checkpoint proteins using a binding assay. As shown in Table 1 and Supporting Information Fig. S2, all interactions, including hCD28/B7-1, hCD28/B7-2, hCTLA4/B7-1, and hCTLA4/B7-2 and LAG3/MHCII, were not affected by YPD-29B (IC_{50} values much higher than 10,000 nmol/L). Altogether, YPD-29B is a highly specific inhibitor of hPD-L1.

3.2. YPD-29B activates T lymphocytes

To explore whether YPD-29B can activate T lymphocytes and overcome immunity tolerance by disrupting the hPD-1/PD-L1 interaction, we performed a PD-L1 cell assay using a TCR activator/PD-L1 HEK293 cell model and a PD-1/NFAT reporter-Jurkat cell system (Fig. 2A). YPD-29B could significantly activate PD-1/NFAT reporter-Jurkat cells in a dose-dependent manner, which was much more effective than BMS202, a known small molecular PD-L1 inhibitor[18,19]. Another positive control, the anti-PD-L1 neutralizing antibody, also effectively stimulated PD-1/NFAT reporter-Jurkat cells, which was comparable to YPD-29B. Furthermore, we investigated the T cell response to YPD-29B by detecting IFN-γ levels. T cells circulating in PBMC were activated by 1 μg/mL PHA as reflected by increased IFN-γ secretion. This activation could be blocked by the recombinant hPD-L1 protein. Interestingly, 10 nmol/L or higher concentrations of YPD-29B significantly rescued T cell inhibition, which was induced by the hPD-L1 protein in a dose-dependent manner, which was also observed by adding anti-PD-L1 antibody (Fig. 2B).

3.3. YPD-29B induces internalization and degradation of PD-L1

It is known that the PD-L1 antibody binds to PD-L1 on the cell surface and leads to subsequent PD-L1 internalization[20]. To explore whether YPD-29B had a similar function as PD-L1 antibody, we evaluated the occupancy ratio in hPD-L1 MC38 cells (Fig. 3A). Indeed, the occupying ratio of PD-L1 increased much more significantly after anti-PD-L1 treatment, similar effects were observed in YPD-29B treated cells in a dose-dependent manner, such capacity to induce PD-L1 internalization of YPD-29 was much stronger than BMS202. Meanwhile, membrane and cytoplasm proteins were extracted from hPD-L1 MC38 cells exposed to YPD-29B. We found that membrane-anchored PD-L1 was negatively regulated while PD-L1 distribution in the cytoplasm increased with YPD-29B treatment (Fig. 3C), suggesting that YPD-29B could efficiently induce internalization of PD-L1 in cancer cells. This was further confirmed by the immunofluorescence staining assay (Fig. 3D). With YPD-29B treatment, PD-L1 protein on the cell membrane decreased significantly, and cytoplasmic PD-L1 expression was increased. Meanwhile, the total expression of PD-L1 in hPD-L1 MC38 cells decreased after treatment with YPD-29B (Fig. 3E), which was consistent with the results obtained in the tumor tissue samples of the animal experiments (Fig. 7E). The PD-L1 protein will be degraded in proteasomes or lysosomes *via* autophagy. We used the proteasome inhibitor MG132 and the lysosomal inhibitor chloroquine (CQ) to treat hPD-L1 MC38 cells. The expression of PD-L1 increased with MG132 and chloroquine treatments, which indicated that in hPD-L1 MC38 cells the PD-L1 protein was degraded in both the proteasomes and the lysosome pathways. With MG132, YPD-29B still induced PD-L1 degradation; however, in the presence of the chloroquine lysosomal inhibitor, YPD-29B could no longer decrease PD-L1 expression (Fig. 3F). Altogether, the data indicated that YPD-29 induced PD-L1 degradation in the lysosomes but not *via* the proteasome pathway.

3.4. YPD-29B induces PD-L1 dimerization

Next, we questioned how YPD-29B interacted with PD-L1 and caused internalization of PD-L1. The HTRF assay (Fig. 4A) was performed to examine whether YPD-29B could induce the dimerization of PD-L1. Our data indicated that YPD-29B was superior to BMS202 in terms of inducing PD-L1 dimerization, with EC_{50} values of 94.8 nmol/L and 1740 nmol/L, respectively (Fig. 4B and C). This finding was further supported by the native PAGE result (Fig. 4D), of note, the anti-PD-L1 antibody did not induce PD-L1 dimerization according to the PAGE result.

To examine the exact interaction sites between YPD-29B and the human PD-L1 dimer, the structure of YPD-29B was bound to the dimer structure of human PD-L1 (PDB code: 5J8O) using a docking study (Fig. 5A and B). Our data reveal that the residues of TYR56 (Chain A), TYR56 (Chain B), and TYR123 (Chain B) of the PD-L1 dimer showed solid $\pi-\pi$ stacking interactions with YPD-29B, and LYS124 (chain B) as well as ARG125 (chain B) exhibited weak cation$-\pi$ interaction with the 3-pyridyl ring of YPD-29B. Furthermore, there was a salt bridge between the side chain of LYS124 (chain B) and the carboxyl group of YPD-29B. The phenyl

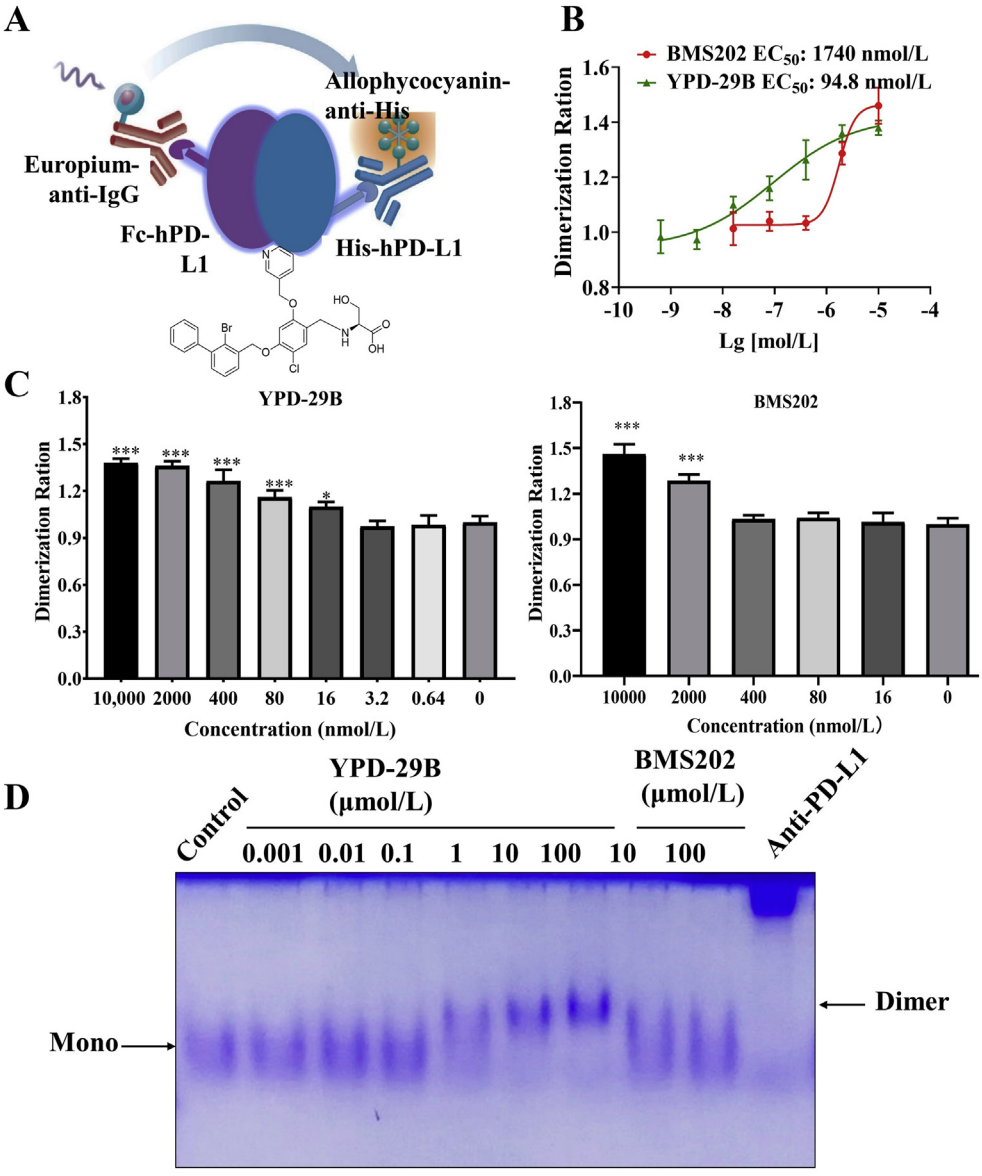

Figure 4 PD-L1 protein dimerization induced by YPD-29B. (A) HTRF experimental scheme. (B) The schematic illustration of PD-L1 protein dimerization induced by YPD-29B. The assays were performed in triplicate at each concentration. Dimerization Ratio = HTRF Ration of compound/HTRF Ration of Control, HTRF Ratio = Signal 665 nm/Signal 615 nm × 10^4. The EC_{50} was calculated using GraphPad using the lg(agonist) *vs*. response−variable slope (four parameters) method. Data are presented as mean ± SD, $n = 3$. (C) YPD-29B increased PD-L1 protein dimerization in the HTRF assay. Different concentrations of YPD-29B or BMS202 were added to the HTRF assay to induce PD-L1 dimerization for 1 h. The dimerization ration was determined and the histogram was prepared using GraphPad software. Data are presented as mean ± SD, $n = 3$; $^*P < 0.05$, $^{**}P < 0.01$, $^{***}P < 0.001$ *vs*. control. (D) YPD-29B increased PD-L1 protein dimerization by native page assay. Indicated compounds with different concentration were incubated with 1 μg PD-L1 for 1 h. The treatment proteins were loaded to native PAGE and then the gel was stained with Coomassie brilliant blue.

ring of YPD-29B was surrounded by the hydrophobic cavity formed by residues ILE54 (chain B), TYR56 (chain B), MET115 (chain B), ALA121 (chain A), TYR123 (chain A), ALA121 (chain B), MET115 (chain A), and ILE54 (chain A). All interactions between the YPD-29B and the hPDL1 dimer ensured strong binding.

3.5. *Evaluation of in vivo antitumor activity of YPD-29B*

Although YPD-29B exhibited potent activity by targeting PD-L1 *in vitro*, but during drug chemistry, manufacturing, and controls (CMC), YPD-29B encountered intractable concerns[21]. Therefore, we modified YPD-29B to the ester prodrug form, YPD-30 (IMMH-010) (Fig. 6A). HTRF results indicated that the IC_{50} value of YPD-30 as PD-L1 inhibitor was 45.2 nmol/L, which was lower than YPD-29B (IC_{50} 1.1 nmol/L). In addition, a cell-based experiment was conducted to compare the activities of the two compounds (Fig. 6C). When the concentration of YPD-30 reached more than 1 μmol/L, the T cells (PBMC) could be activated to produce IFN-γ. However, YPD-29B could activate T cells starting at a concentration of 10 nmol/L, which was much stronger than

YPD-30. Importantly, since YPD-29B did not block the interaction between mouse PD-1 and PD-L1 (Suporting Information Fig. S3), we then evaluated the affinities of YPD-29B to various PD-L1 protein forms from different species. As shown in Table 2, the K_D values of YPD-29B for the rat, cynomolgus monkey, and human PD-L1 protein were 2.77×10^{-8}, 8.64×10^{-11}, and 3.67×10^{-11} mol/L, respectively, suggesting that YPD-29B was more affinitive to the cynomolgus monkey and human. Thus, we implanted hPD-L1 MC-38 cells in humanized hPD-1 mice to assess the antitumor activity of YPD-30 *in vivo* (Fig. 6D). Mice received oral YPD-30 at doses of 2.5, 5, and 10 mg/kg every day, while hPD-L1 antibody was administered intraperitoneally at a dose of 10 mg/kg twice a week. We observed that tumor progression was significantly delayed in YPD-30 treated mice in a dose-dependent manner compared to the vehicle group (Fig. 6E). Tumor growth inhibitions (TGI) in the YPD-30 groups were 40.5% (2.5 mg/kg), 60.9% (5 mg/kg), and 67.9% (10 mg/kg), respectively, while anti-PD-L1 TGI was 72.0% (Fig. 6F, Supporting Information Table S1). The body weight of the mice treated with YPD-30 increased steadily as the vehicle group throughout the experiments (Fig. 6G).

Next, we evaluated T lymphocyte infiltration in different treated mice. As expected, the infiltration of $CD3^+CD4^+$ and $CD3^+CD8^+$ T cells into tumors was markedly increased (Fig. 7A–C). Similarly, $CD3^+CD8^+$ T cells were also elevated in blood collected from YPD-30 treated mice (Supporting Informaiton Fig. S4B). Meanwhile, the spleen index and the thymus index of mice showed an increasing trend after administration of YPD-30 (Fig. S4A). These phenomena indicated that the immune systems of mice were activated by YPD-30. Since active YPD-29B caused internalization of PD-L1, we also analyzed the *in vivo* binding ratio of hPD-L1 in tumors exposed to YPD-30. Consistent with the *in vitro* results, YPD-30 indeed significantly reduced the fluorescence intensity of PD-L1, especially in mice treated with 10 mg/kg YPD-30 (Fig. 7D and E). A similar result was observed in the anti-PD-L1 antibody treatment group. Importantly, the protein levels of hPD-L1 in tumor tissues were down-regulated upon YPD-30 treatment (Fig. 7F). Furthermore, immunohistochemical staining of an independent set of tumor tissues showed that YPD-30 significantly increased T cell infiltration by increasing CD3 and CD8 expression in the anti-PD-L1 treatment group (Fig. 8A and B). Meanwhile, hPD-L1 expression was markedly decreased by YPD-30 and antibody treatment (Fig. 8A and B). Taken together, our data indicated that YPD-30, the prodrug of YPD-29B, showed great antitumor activity by inhibiting PD-L1 *in vivo*.

4. Discussion

Unlike chemotherapy, cancer immunotherapy has represented a breakthrough approach for cancer treatment[22]. Among various immunotherapy methods, immune checkpoint inhibitors hold a prominent role[23,24]. At present, all the currently available immune checkpoint inhibitors are antibodies[25]. Although they exhibited excellent clinical efficacy, there are also many limitations. Immune-related adverse events (irAEs) arise during clinical application. Due to a long half-life and high target occupancy, irAEs especially grade 3 and 4 adverse events cannot be easily resolved despite treatment cessation[26,27]. Furthermore, the clinical response rates are not as high as expected. One reason is that antibodies have a limited ability to penetrate to the inner regions of the tumor. Small molecular inhibitors target immune checkpoints, exhibiting the potential to overcome the shortcomings of antibody-based checkpoint inhibitors. In addition, small molecular inhibitors can be administered orally compared to intravenous injection of antibodies. Furthermore, the short half-life of small molecular molecules will benefit the management of irAEs and provide more potential for treatment combinations[28].

The first series of small molecule compounds from Bristol-Myers Squibb (BMS) is still in pre-clinical research, and include BMS202 and BMS1166[29]. In addition, small molecules targeting PD-L1 and VISTA (CA-170) or TIM3 (CA-327) are currently

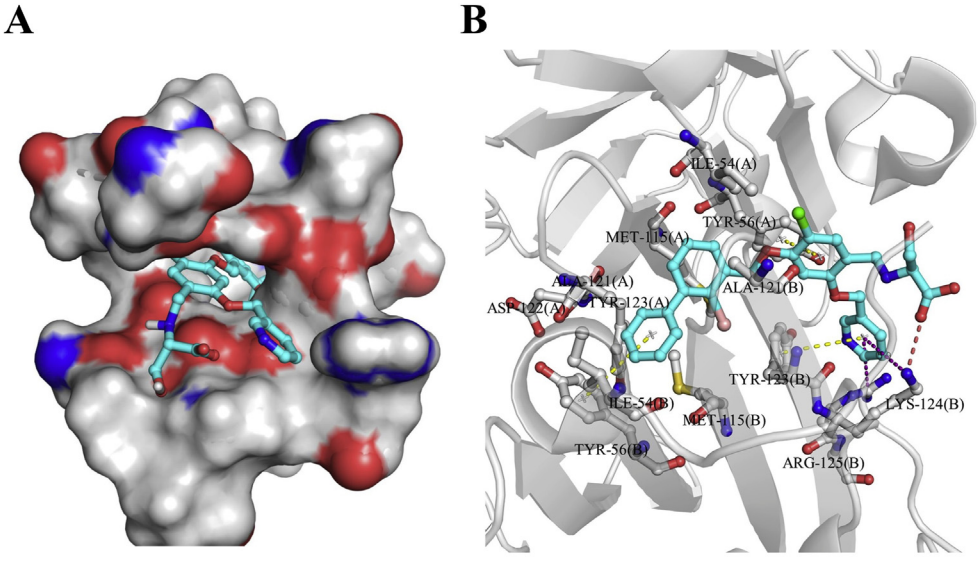

Figure 5 Predicted binding modality of YPD-29B with hPD-L1. (A) YPD-29B in the PD-L1 dimer binding pocket. (B) The binding conformations of compound YPD-29B in the active site of protein. Compound YPD-29B is shown as a cyan stick structure and the surrounding residues are gray. $\pi-\pi$ stacking interactions are in yellow dotted lines and anion$-\pi$ interactions are in purple dotted lines, and the salt bridge is in orange dotted line.

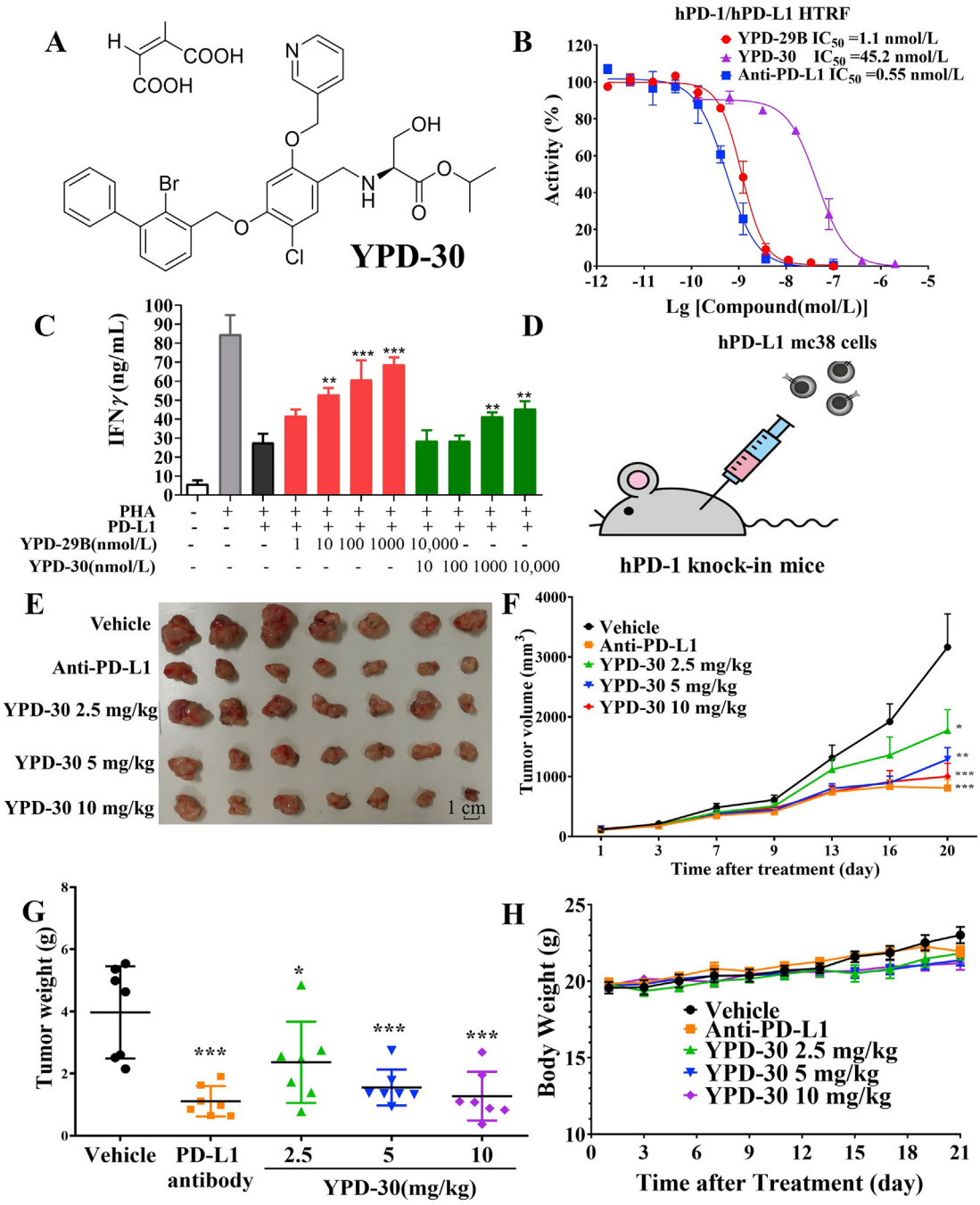

Figure 6 The antitumor activity of YPD-30 *in vivo*. (A) Chemical structure of YPD-30. (B) YPD-30 interrupts the hPD-1/hPD-L1 interaction as shown by the HTRF assay. (C) YPD-30 weakly activates T cells. The PBMC cells were treated with or without PHA (1 μg/mL) and PD-L1 (5 μg/mL). Then different concentrations of YPD-29B or YPD-30 were used to treat the cells for 72 h, and the IFN-γ in the supernatant was determined by ELISA ($n = 3$). Data are presented as mean ± SD, $^{*}P < 0.05$, $^{**}P < 0.01$, $^{***}P < 0.001$ *vs*. the group only with PHA and PD-L1 (in black). (D) Diagram of double humanization mouse model. In this model, the expression of mouse PD-L1 in the mouse colon MC38 cancer cells is knocked out and then human PD-L1 is knocked in. In addition, the PD-1 protein in the tumor bearing mouse is humanized. (E) Images of the stripped tumor ($n = 7$). On Day 21, the mice were euthanized and the tumor tissue was excised and then photographed. (F) The growth curve of tumor volume ($n = 7$). The tumor volume is measured on Days 1, 3, 7, 9, 13, 16, 20. Quantitative data are presented as mean ± SD, $^{*}P < 0.05$, $^{**}P < 0.01$; $^{***}P < 0.001$ *vs*. vehicle. (G) The inhibitory effect of YPD-30 on tumor weight ($n = 7$). Quantitative data was presented as mean ± SD, $^{*}P < 0.05$, $^{**}P < 0.01$, $^{***}P < 0.001$ *vs*. vehicle. (H) The body weight of each group ($n = 7$). Mice weight was measured every day and the quantitative data are presented as mean ± SD.

being tested in clinical trials[30,31]. CA-170 has completed a first-in-human phase I trial. Clinical data suggested that CA-170 has an acceptable safety profile and the results from a small population of patients showed preliminary signs of antitumor activity, including tumor shrinkage and a prolonged stable disease. However, evidence showed that there was no direct binding between CA-170

Table 2 The affinity of YPD-29B in different species of PD-L1.

Affinity	Rat		*Cynomolgus* monkey		Human	
	YPD-29B	rPD-L1mab	YPD-29B	cmPD-L1mab	YPD-29B	hPD-L1mab
K_a (1/ms)	2.02×10^{-5}	6593	2.34×10^{-6}	7.15×10^{-4}	1.53×10^{-6}	3.28×10^{-6}
K_d (1/s)	5.59×10^{-3}	5.60×10^{-4}	2.02×10^{-4}	5.74×10^{-4}	5.60×10^{-5}	2.82×10^{-4}
K_D (mol/L)	2.77×10^{-8}	8.49×10^{-8}	8.64×10^{-11}	8.03×10^{-9}	3.67×10^{-11}	8.58×10^{-11}
R_{max} (RU)	5.33	306.10	27.18	94.82	31.99	47.28

and PD-L1[30]. Another oral small molecular PD-L1 inhibitor from Incyte, INCB86550, is also being tested in clinical trials[32]. These data indicated that small inhibitors targeting immune checkpoints have potential for cancer immunotherapy. However, the efficacy and safety of small inhibitors are still required for clinical testing in large numbers of cancer patients.

Here, we develop and test a small molecular, YPD-29B, targeting PD-L1. YPD-29B showed potent and selective activity targeting human PD-L1 *in vitro*. As shown in Table 2, the K_D values of YPD-29B for rat, cynomolgus monkey, and human PD-L1 protein were 2.77×10^{-8}, 8.64×10^{-11}, and 3.67×10^{-11} mol/L, respectively. In addition, as shown in Table 1, YPD-29B does not bind to mouse PD-L1, as also further confirmed by the SPR assay (data not shown). All data indicated that the affinity of YPD-29B to PD-L1 decreased from mammals to rodents and with no affinity to mouse PD-L1. We verified the amino acid sequence of different species of PD-L1 protein using PubMed. The amino acid sequence of the extracellular domain of human PD-L1 was 96%, 73%, and 72% homologous to monkey cynomolgus, rat, and mouse PD-L1, respectively. Thus, it is easy to understand that YPD-29B shows an extremely high affinity for human and cynomolgus monkey PD-L1. We also evaluated the homology of the rat and mouse extracellular domain of PD-L1; only 85% identity was observed. We speculated that the rat protein retained several important amino acids required for binding to YPD-29B, which were not present in the mouse protein. Indeed, coupling data indicated that an important amino acid, MET115, was missing in the mouse protein, which was necessary to form the hydrophobic cavity necessary for the binding of YPD-29B to PD-L1 protein. To better understand the binding of the YPD-29B and PD-L1 proteins, we are currently analyzing the crystal structures of the YPD-29B/hPD-L1 complex in collaboration with Shuimu Bioscience of Tsinghua University.

The T cell activation data (Fig. 2A) show that YPD-29B at the highest concentration tested (25 μmol/L) did not match the efficacy of treatment with the PD-L1 antibody. In addition, in the rescue assay evaluating IFN-γ induction in human PBMC, a dose of 2000 nmol/L YPD-29B showed less efficacy than the 10 nmol/L PD-L1 antibody. However, as shown in Fig. 1 and Table 1, YPD-29B shows greater affinity and selectivity for PD-L1 than the PD-L1 antibody. There was an obvious discrepancy between the protein and cell-based assay. We also found that the small molecule BMS202 inhibitor presented a similar incongruity. BMS-202 could inhibit the interaction of PD-1/PD-L1 with an IC_{50} of 18 nmol/L, but in the T cell activation assay, more than 10 μmol/L of BMS202 was required. We speculated that this could be attributed to differences in the purified PD-L1 protein and the endogenous structure of the transmembrane protein. This difference may be caused by glycosylation, acylation, or other post-translational modifications. This modification has little effect on the strong binding of antibody complementary determinants and antigen epitopes. However, the formation of the PD-L1 dimer is required before YPD-29B can bind to the complex. Any glycosylation, acylation, or other post-translational modification preventing dimerization would also preclude YPD-29B binding. The effect of this modification on the formation of the PD-L1 dimer has been discussed in the literature reported by Zak et al.[33]. As mentioned above, a study is currently underway to analyze the crystal structures of the YPD-29B/PD-L1 complex in collaboration with Shuimu Bioscience of Tsinghua University. Once the key amino acids for the YPD-29B/PD-L1 complex are identified, this will allow the study of the post-translational modification of these amino acids, which will undoubtedly lead to the development of a new generation of PD-L1 small molecules.

Furthermore, YPD-29B could activate T lymphocytes in a dose-dependent manner by inducing dimerization and internalization of PD-L1 *in vitro*. Thus, humanized PD-1 mice implanted with humanized PD-L1 mice were established for the *in vivo* pharmacodynamics assay. Furthermore, YPD-29 is too hygroscopic to be formulated for use as a pharmaceutical compound. Thus, the carboxylic acid of YPD-29B was masked, generating the ester prodrug YPD-30. This prodrug strategy may improve the druggability of YPD-29B. Pharmacokinetics studies showed that the transformation of YPD-30 in liver S9 of mouse, rat, dog, monkey, and human were all complete (100% transformation) within 40 min. After oral administration, compound YPD-30 was easily transformed into YPD-29B in mouse plasma and then achieved higher exposure in tumor tissues[21]. Next, we assessed its therapeutic effects on humanized hPD-1 mice implanted with hPD-L1 MC38 cells. Daily oral administration of YPD-30 exhibited strong antitumor activities *in vivo* with decreased expression of PD-L1 and increased infiltration of T lymphocytes in tumor. BMS202 has been reported to present a 50.1% inhibition rate in B16F10 tumor with a dose of 60 mg/kg[18] and a 41% inhibition rate in humanized mouse-transplanted human SCC-3 tumor with a dose of 20 mg/kg[19]. In contrast, YPD-30 showed greater efficacy at a lower dose (10 mg/kg) and achieved much more significant efficacy, reaching a 67.9% inhibition rate. Furthermore, compared to compound BMS202, YPD-29B showed no toxicity to normal human cells or cancer cells (Supporting Information Table S2). Therefore, the activity of YPD-30 (YPD-29B) was significantly superior to that of BMS202, both in our *in vitro* assays and in *in vivo* assays reported by other groups[19,33]. Whereas, only $CD8^+$ T lymphocytes exhibited significant upregulation in blood with YPD-30 administration. There were no significant changes in $CD4^+$ T lymphocytes in the YPD-30 and PD-L1 antibody treatment groups. Furthermore, during treatment, the body weight of the mice in the YPD-30 groups increased and no serious adverse reactions were observed. In the repeated-dose cytotoxicity study, we again did not observe any serious adverse effects in Sprague−Dawley rats and Cynomolgus monkey (data not shown). Pathological changes were observed in different organs after treatment with YPD-30. Only after a large dose of 1000 mg/kg for 4 weeks there was evidence of an obvious

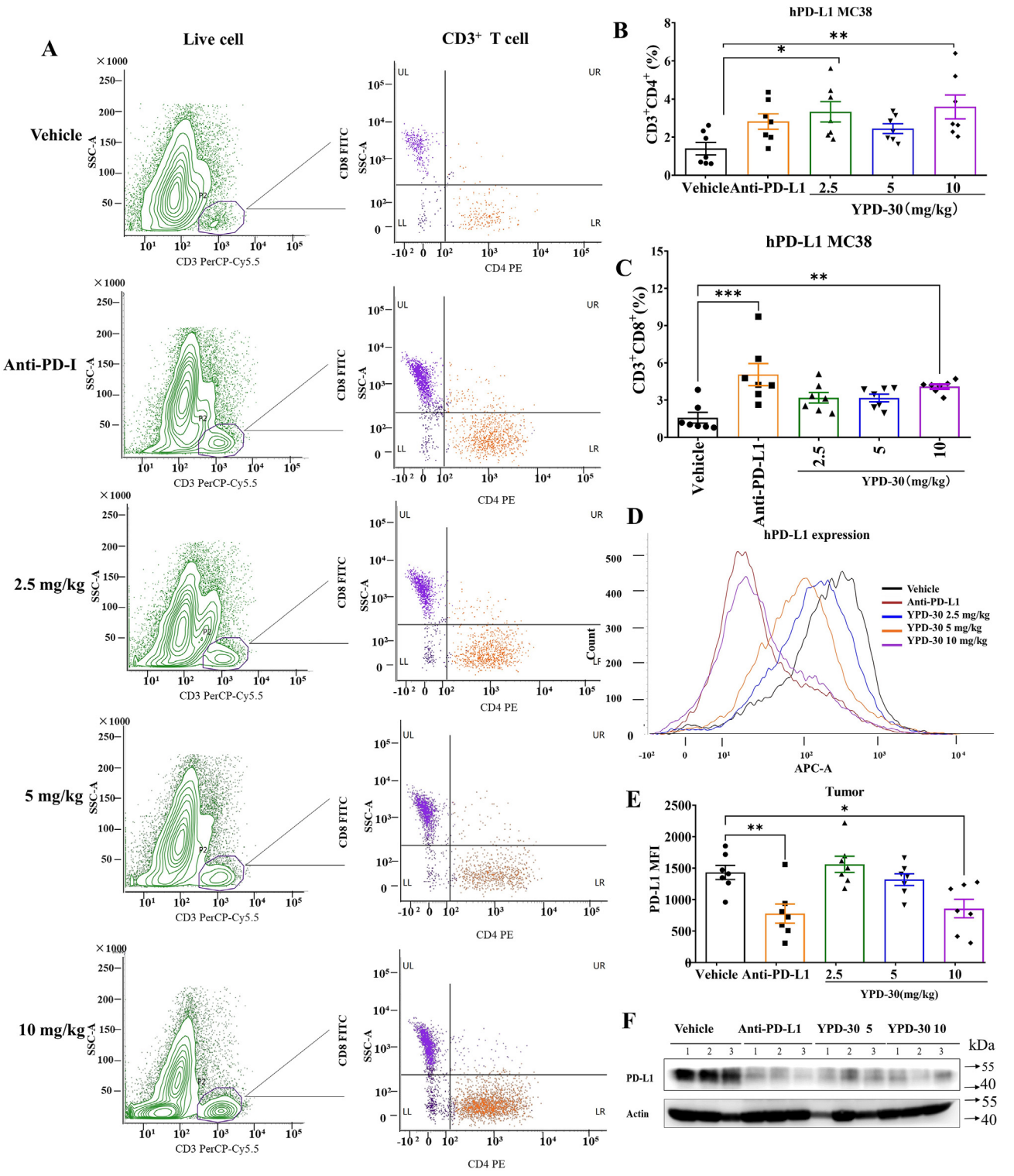

Figure 7 The antitumor mechanism of YPD-30 *in vivo*. (A) Multicolor flow cytometry images of different groups treated by YPD-30. The tumors were homogenized to single cell suspensions and subjected to PerCP-Cy5.5-CD3$^+$, PE-CD4$^+$, FITC-CD8$^+$ and APC-PD-L1 staining for 1 h. First the positive PerCP-CY5.5-CD3$^+$ cells from the total living cells are circled as P2 gate, and then PE-CD4$^+$, FITC-CD8$^+$ from CD3$^+$ cells are distinguished. (B) CD3$^+$CD4$^+$ tumor infiltrated T lymphocytes in tumor tissues. The proportion of CD3$^+$CD4$^+$ cells in the total living cells were shown. Quantitative data are presented as mean ± SD (n = 7). *P < 0.05, **P < 0.01, ***P < 0.001 *vs*. vehicle. (C) CD3$^+$CD8$^+$ tumor infiltrated T lymphocytes in tumor tissues. The proportion of CD3$^+$CD8$^+$ cells in the all living cells is shown. Quantitative data are the mean ± SD (n = 7), *P < 0.05, **P < 0.01, ***P < 0.001 *vs*. vehicle. (D) PD-L1 expression of the tumor cells is decreased by YPD-30. The representative data of each group is shown. (E) Membrane PD-L1 expression of tumor cells were decreased by YPD-30. The quantitative data of each group are presented as mean ± SD (n = 7), *P < 0.05, **P < 0.01 *vs*. indicated. (F) Total PD-L1 expression is decreased by YPD-30. The tumors were homogenized and subjected to Western blotting for PD-L1 expression. A representative Western blot is shown (n = 3). Quantitative data are presented as mean ± SD, *P < 0.05, **P < 0.01, ***P < 0.001 *vs*. vehicle control.

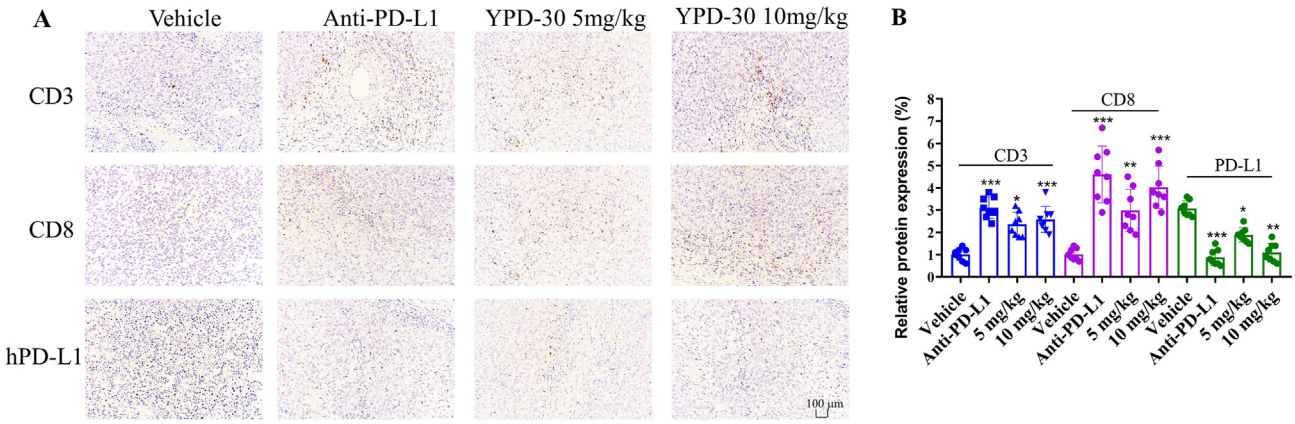

Figure 8 The antitumor mechanism of YPD-30 *in vivo* by immunohistochemical staining. (A) $CD3^+$, $CD8^+$ and hPD-L1 in hPD-L1 MC38 xenograft tumor tissue was collected and subjected to immunohistochemical staining with specific antibodies. Scale bar = 10 μm. (B) Quantification of $CD3^+$, $CD8^+$ and hPD-L1 expression in tumor tissue ($n = 8$). $^*P < 0.05$, $^{**}P < 0.01$ and $^{***}P < 0.001$ *vs*. indicated.

inflammatory reaction in the rat heart; however, this dose was much higher than the therapeutic dose of 10 mg/kg. All the data show that the immune-related side effects of PD-L1 small molecule were attenuated, indicating that small molecular inhibitor YPD-30 is better tolerated orally and exhibits a good safety profile.

5. Conclusions

We developed a potent and selective small molecular YPD-29B targeting human PD-L1, which can down-regulate levels of PD-L1 by inducing PD-L1 dimerization and internalization, further activating T lymphocytes. Its prodrug, YPD-30, exhibits profound antitumor activity and is well tolerated *in vivo*, which may serve as a therapeutic agent for cancer therapy.

Acknowledgments

This work was supported by the National Natural Science Foundation of China (No. 81872923), the CAMS Innovation Fund for Medical Sciences (2016-I2M-3-008, China) and The Drug Innovation Major Project (No. 2018ZX09711001-003, China).

Author contributions

Fangfang Lai and Ming Ji carried out most of the experiments and wrote the manuscript. Yunchen Wang and Nina Xue helped the animal experiments. Lei Huang and Tingting Du contributed to the data analysis. Kai Dong and Xiaoqing Yao mainly helped provide experimental ideas and suggestions for modification. Jing Jin, Zhiqiang Feng and Xiaoguang Chen designed the whole study and revised the manuscript. All authors read and approved the final manuscript.

Conflicts of interest

The authors declare that there is no conflict of interest.

Appendix A. Supporting information

Supporting data to this article can be found online at https://doi.org/10.1016/j.apsb.2022.02.031.

References

1. Sukari A, Nagasaka M, Al-Hadidi A, Lum LG. Cancer immunology and immunotherapy. *Anticancer Res* 2016;**36**:5593−606.
2. Feins S, Kong W, Williams EF, Milone MC, Fraietta JA. An introduction to chimeric antigen receptor (CAR) T-cell immunotherapy for human cancer. *Am J Hematol* 2019;**94**:S3−9.
3. Korman A, Yellin M, Keler T. Tumor immunotherapy: preclinical and clinical activity of anti-CTLA4 antibodies. *Curr Opin Investig Drugs* 2005;**6**:582−91.
4. Kiaie SH, Sanaei MJ, Heshmati M, Asadzadeh Z, Azimi I, Hadidi S, et al. Immune checkpoints in targeted-immunotherapy of pancreatic cancer: new hope for clinical development. *Acta Pharm Sin B* 2021;**11**:1083−97.
5. Lee JJ, Chu E. Recent advances in the clinical development of immune checkpoint blockade therapy for mismatch repair proficient (PMMR)/non-MSI-H metastatic colorectal cancer. *Clin Colorectal Cancer* 2018;**17**:258−73.
6. Mehrvarz Sarshekeh A, Overman MJ, Kopetz S. Nivolumab in the treatment of microsatellite instability high metastatic colorectal cancer. *Future Oncol* 2018;**14**:1869−74.
7. Flynn MJ, Larkin JMG. Novel combination strategies for enhancing efficacy of immune checkpoint inhibitors in the treatment of metastatic solid malignancies. *Expert Opin Pharmacother* 2017;**18**:1477−90.
8. Kon E, Benhar I. Immune checkpoint inhibitor combinations: current efforts and important aspects for success. *Drug Resist Updat* 2019;**45**:13−29.
9. Yang W, Li S, Yang Q. Risk of dermatologic and mucosal adverse events associated with PD-1/PD-L1 inhibitors in cancer patients: a meta-analysis of randomized controlled trials. *Medicine (Baltimore)* 2019;**98**:e15731.
10. Wang L, Ma Q, Yao R, Liu J. Current status and development of anti-PD-1/PD-L1 immunotherapy for lung cancer. *Int Immunopharmacol* 2020;**79**:106088.
11. Basu S, Yang J, Xu B, Magiera-Mularz K, Skalniak L, Musielak B, et al. Design, synthesis, evaluation, and structural studies of C_2-symmetric small molecule inhibitors of programmed cell death-1/programmed death-ligand 1 protein−protein interaction. *J Med Chem* 2019;**62**:7250−63.
12. Kopalli SR, Kang TB, Lee KH, Koppula S. Novel small molecule inhibitors of programmed cell death (PD)-1, and its ligand, PD-L1 in cancer immunotherapy: a review update of patent literature. *Recent Pat Anticancer Drug Discov* 2019;**14**:100−12.
13. Li K, Tian H. Development of small-molecule immune checkpoint inhibitors of PD-1/PD-L1 as a new therapeutic strategy for tumour immunotherapy. *J Drug Target* 2019;**27**:244−56.

14. Sasikumar PG, Ramachandra M. Small-molecule immune checkpoint inhibitors targeting PD-1/PD-L1 and other emerging checkpoint pathways. *BioDrugs* 2018;**32**:481−97.
15. Shaabani S, Huizinga HPS, Butera R, Kouchi A, Guzik K, Magiera-Mularz K, et al. A patent review on PD-1/PD-L1 antagonists: small molecules, peptides, and macrocycles (2015−2018). *Expert Opin Ther Pat* 2018;**28**:665−78.
16. Lee JJ, Powderly JD, Patel MR, Brody J, Hamilton EP, Infante JR, et al. Phase 1 trial of CA-170, a novel oral small molecule dual inhibitor of immune checkpoints PD-1 and vista, in patients (PTS) with advanced solid tumor or lymphomas. *J Clin Oncol* 2017;**35**: TPS3099.
17. Jin J, Xue N, Liu Y, Fu R, Wang M, Ji M, et al. A novel S1P1 modulator IMMH002 ameliorates psoriasis in multiple animal models. *Acta Pharm Sin B* 2020;**10**:276−88.
18. Hu Z, Yu P, Du G, Wang W, Zhu H, Li N, et al. PCC0208025 (BMS202), a small molecule inhibitor of PD-L1, produces an anti-tumor effect in B16-F10 melanoma-bearing mice. *PLoS One* 2020;**15**: e0228339.
19. Ashizawa T, Iizuka A, Tanaka E, Kondou R, Miyata H, Maeda C, et al. Antitumor activity of the PD-1/PD-L1 binding inhibitor BMS-202 in the humanized MHC-double knockout NOG mouse. *Biomed Res* 2019;**40**:243−50.
20. Wang Y, Wang H, Yao H, Li C, Fang JY, Xu J. Regulation of PD-L1: emerging routes for targeting tumor immune evasion. *Front Pharmacol* 2018;**9**:536.
21. Wang Y, Liu X, Zou X, Wang S, Luo L, Liu Y, et al. Metabolism and interspecies variation of IMMH-010, a programmed cell death ligand 1 inhibitor prodrug. *Pharmaceutics* 2021;**13**:598.
22. Yang Y. Cancer immunotherapy: harnessing the immune system to battle cancer. *J Clin Invest* 2015;**125**:3335−7.
23. Haanen JB, Robert C. Immune checkpoint inhibitors. *Prog Tumor Res* 2015;**42**:55−66.
24. Ni L, Dong C. New checkpoints in cancer immunotherapy. *Immunol Rev* 2017;**276**:52−65.
25. Balar AV, Weber JS. PD-1 and PD-L1 antibodies in cancer: current status and future directions. *Cancer Immunol Immunother* 2017;**66**: 551−64.
26. Li B, Chan HL, Chen P. Immune checkpoint inhibitors: basics and challenges. *Curr Med Chem* 2019;**26**:3009−25.
27. Foller S, Oppel-Heuchel H, Fetter I, Winkler Y, Grimm MO. Adverse events of immune checkpoint inhibitors. *Urologe A* 2017;**56**: 486−91.
28. Zhan MM, Hu XQ, Liu XX, Ruan BF, Xu J, Liao C. From monoclonal antibodies to small molecules: the development of inhibitors targeting the PD-1/PD-L1 pathway. *Drug Discov Today* 2016;**21**:1027−36.
29. Guzik K, Zak KM, Grudnik P, Magiera K, Musielak B, Torner R, et al. Small-molecule inhibitors of the programmed cell death-1/programmed death-ligand 1 (PD-1/PD-L1) interaction *via* transiently induced protein states and dimerization of PD-L1. *J Med Chem* 2017;**60**:5857−67.
30. Musielak B, Kocik J, Skalniak L, Magiera-Mularz K, Sala D, Czub M, et al. CA-170—a potent small-molecule PD-L1 inhibitor or not?. *Molecules* 2019;**24**:2804.
31. Tagliamento M, Bironzo P, Novello S. New emerging targets in cancer immunotherapy: the role of VISTA. *ESMO Open* 2020;**4**:e000683.
32. Yang M, Liang C, Swaminathan K, Herrlinger S, Lai F, Shiekhattar R, et al. A C9ORF72/SMCR8-containing complex regulates ULK1 and plays a dual role in autophagy. *Sci Adv* 2016;**2**:e1601167.
33. Zak KM, Grudnik P, Guzik K, Zieba BJ, Musielak B, Domling A, et al. Structural basis for small molecule targeting of the programmed death ligand 1 (PD-L1). *Oncotarget* 2016;**7**:30323−35.